



1

2

3

## 4 Characterization of Hillslope Hydrologic Events through a Self-Organizing Map

5

6

7

8 Eunhyung Lee and Sanghyun Kim

9 Department of Environmental Engineering, College of Engineering, Pusan National University,

10 Busan, South Korea

11 Corresponding author: Sanghyun Kim ([kimsangh@pusan.ac.kr](mailto:kimsangh@pusan.ac.kr))

12

13

14

15

16

### 17 **Key Points:**

18 Hydrologic events in a hillslope were analyzed using self-organizing map.

19 The maximum variation and response time of soil moisture are useful in process-based event  
20 identification.

21 Combinations of hillslope hydrological processes were responsible for five delineated event  
22 clusters.

23



24 **Abstract**

25 Hydrologic events can be characterized as particular combinations of hydrological processes on a  
26 hillslope scale. To configure hydrological mechanisms, we analyzed a dataset using an  
27 unsupervised machine learning algorithm to cluster the hydrologic events based on the  
28 dissimilarity distances between the weighting components of a self-organizing map (SOM). The  
29 time series of soil moisture was measured at 30 points (in 10 locations with 3 varying depths) for  
30 356 rainfall events on a steep, forested hillslope between 2007 and 2016. Soil moisture features  
31 for hydrologic events can be effectively represented by the antecedent soil moisture, maximum  
32 variation, and standard deviation of peak-to-peak time between rainfall and soil moisture response.  
33 Five clusters were delineated for hydrologically meaningful event classification in the SOM  
34 representation. The two-dimensional spatial weighting patterns in the SOM provided greater  
35 insight on relationships between rainfall characteristics, antecedent wetness, and soil moisture  
36 response at different locations and depths. The distinction of the classified events can be explained  
37 by several rainfall features and antecedent soil moisture conditions that resulted in different  
38 patterns made by combinations of hillslope hydrological processes, vertical flow, and lateral flow  
39 along either surface or subsurface boundaries for the upslope and downslope areas.

40

41 **Keywords:** rainfall, soil moisture, hillslope hydrology, self-organizing map, process-based  
42 characterization

43

44

45

46



## 47 **1 Introduction**

48 Soil moisture information is critical for assessing water storage, estimating the quantity of runoff  
49 generated, and determining slope stability for hillslopes during rainfall (Tromp Van Meerveld and  
50 McDonnel, 2005; Lu and Godt, 2008; Penna et al., 2011; Angermann et al., 2017). Hillslope  
51 hydrological processes are affected by many factors, including topography, soil texture, and eco-  
52 hydrological parameters (Western et al., 1999; Rodriguez-Iturbe et al., 2006; Liang et al., 2011;  
53 Rosenbaum et al., 2012; Baroni et al., 2013), which results in highly nonstationary and  
54 heterogeneous spatiotemporal distributions of soil moisture (Wilson et al., 2004; Penna et al.,  
55 2009). The relationship between precipitation and runoff is highly nonlinear, and the  
56 spatiotemporal variations in soil moisture, groundwater, and surface runoff are extremely difficult  
57 to predict (Ali et al., 2013; Curtu et al., 2014).

58         Rainfall is the primary driver of rapid variations in soil moisture and subsurface flow  
59 generation (Penna et al., 2011). Soil moisture response to rainfall events has been investigated for  
60 various topographic positions, depth profiles, and land cover conditions (He et al., 2012; Wang et  
61 al., 2013; Zhu et al., 2014; Feng and Liu, 2015). The functional relationship between rainfall events  
62 and soil moisture, depends on various factors, such as soil texture, depth, topography, and  
63 vegetation cover (Liang et al., 2011; Bachmair et al., 2012; Gwak and Kim, 2016). Rainfall  
64 characteristics, including the total quantity, duration, intensity, and dry period duration, have also  
65 been used to understand the soil moisture response (Heisler-White et al., 2008; Albertson and  
66 Kiely, 2001). Other studies of rainfall features have categorized rainfall events to analyze soil  
67 moisture variation (Lai et al., 2016; Wang et al., 2008).

68         Antecedent soil moisture (ASM) plays an essential role in the hydrological response at the  
69 hillslope scale (Hardie et al., 2011; Uber et al., 2018; Lee and Kim, 2020). The interaction between



70 the spatial distribution of ASM and rainfall events, determines various hydrological processes,  
71 such as the occurrence of preferential flow, soil moisture variation patterns, subsurface stormflow,  
72 and runoff generation (Bachmair et al., 2012; Zhang et al., 2011; Saffarpour et al., 2016;  
73 Wiekenkamp et al., 2016). The wetter ASM and the greater rainfall events resulted in a greater  
74 variation in soil moisture and deeper rainwater percolation (Zhu et al., 2014; Lai et al., 2016; Lee  
75 and Kim 2020).

76 Due to the generation of distinct hillslope flow paths, vertical flows such as matrix, bypass,  
77 and lateral flows along different boundaries (e.g., subsurface stormflow over bedrock and surface  
78 overland flow) can vary along the transect of the hillslope (Wienhöfer and Zehe, 2014). Previous  
79 studies have investigated the functional relationship between rainfall and soil water storage  
80 (Castillo et al., 2003; Crow and Ryu, 2009; Trambly et al., 2012). However, the influence of  
81 rainfall features such as rainfall amount, intensity, duration, and ASM conditions on the generation  
82 of hillslope flow paths and their distributions at the hillslope scale have not been sufficiently  
83 explored. Other studies on hillslope hydrology have focused on several events to identify specific  
84 flow paths (e.g., subsurface lateral flow) using intensively collected field measurements over  
85 relatively short periods (Freer et al., 2004; Kim 2009; Penna et al., 2011; Wienhöfer and Zehe,  
86 2014).

87 A comprehensive approach can be useful for addressing the holistic behavior of  
88 hydrological processes using a dataset of substantial number of events collected over many years.  
89 Identification of specific hydrological processes through visual inspection of field data can be  
90 labor-intensive, and the accuracy of analysis can be marginal and subjective if the size of the  
91 dataset is large.



92 Machine learning techniques have been applied to soil moisture data from in-situ  
93 measurements (Ley et al., 2011; van Arkel and Kaleita, 2014; Carranza et al., 2021), remote  
94 sensing applications (Ahmad et al., 2010; Srivastava et al., 2013), and the analysis of hydrological  
95 model performance (Shrestha et al., 2009; Herbst et al., 2009). Supervised learning algorithms  
96 have been used to improve predictions of subsurface flow in a hillslope (Bachmair and Weiler,  
97 2012), downscale satellite soil moisture data (Srivastava et al., 2013), and estimate soil moisture  
98 obtained through regression analysis (Ahmad et al., 2010). Critical soil moisture sampling points  
99 have also been identified using unsupervised learning algorithms (Van Arkel and Kaleita, 2014; ;  
100 Liao et al., 2017). Most studies involving machine learning algorithms for the analysis of soil  
101 moisture have focused on estimating and determining the appropriate measurement locations for  
102 assessing variations in mean soil moisture. However, soil moisture response can be further  
103 explored in the context of hydro-meteorological (rainfall), hydro-historic (ASM), and topographic  
104 (location and depth) controllers at the hillslope scale.

105 A self-organizing map (SOM), which is an unsupervised neural network method, has been  
106 used to investigate datasets representing ecosystems, animals, catchment classification, and crop  
107 evapotranspiration (Ley et al., 2011; Casper et al., 2012; Ismail et al., 2012; Farsadnia et al., 2014).  
108 An SOM can be an effective tool for understanding large hydrologic data by reducing the  
109 dimensionality of a dataset, which can provide hydrologic interpretation. Furthermore, and SOM  
110 can be used to successfully address the nonlinear relationship between hydrologic variables (di  
111 Prinzio et al., 2011; Ley et al., 2011; Toth, 2013; Chen et al., 2018). The highly heterogeneous and  
112 extremely nonstationary variation in soil moisture between the upslope and downslope areas  
113 alongside the upper, middle, and lower soil layers of a hillslope can be analyzed using an SOM.

114 In this study, we aimed to answer the following research questions:



115 1. How can machine learning algorithms be used to understand the soil moisture response  
116 patterns at the hillslope scale?

117 2. Can delineated clusters of hydrologic events be explained by different hillslope  
118 hydrological processes?

119 In this study, an alternative method for understanding hillslope hydrologic behavior was  
120 explored through long-term data analysis using SOM. Hydrologic events for the hillslope scale  
121 can be characterized through the rigorous classification of a large hydrologic dataset. Particularly,  
122 machine learning algorithms provide several opportunities for understanding hydrologic events by  
123 transforming a substantial dataset into compact clusters and delineating the hierarchical  
124 relationship between clusters, which can be useful for exploring process-based interpretations and  
125 obtaining an efficient monitoring network. We used hydrologic data (rainfall and soil moisture) to  
126 analyze and characterize the highly complex relationships between ASM, rainfall characteristics,  
127 and soil moisture responses, which include variation in soil moisture and the time to peak. The  
128 SOM was employed to investigate the nonlinear interactions between various rainfall  
129 characteristics and their effects on temporal changes in soil moisture and classify the multivariate  
130 datasets regarding the likely flow paths in the hillslope.

131 We employed the following approaches to address these research topics: First, we applied  
132 an SOM algorithm to datasets composed of rainfall features, ASM, and soil moisture status from  
133 upslope to downslope locations in the study area. The dataset was reclassified based on the  
134 weighting vectors of each neuron in the SOM map using the Euclidean distances between distinct  
135 hydrological variables from individual hydrologic events. Second, the nonlinear relationship  
136 between rainfall and soil moisture was evaluated by comparing the spatially weighted patterns of  
137 rainfall characteristics and soil wetness variables. The relationships between rainfall characteristics



138 and soil moisture at varying depths and locations were investigated, and these data were used to  
139 interpret the hydrological processes.

140

## 141 **2 Materials and Methods**

142

### 143 **2.1 Study Area and Data Acquisition**

144 The hillslope (4000 m<sup>2</sup>) selected for the study, is in the Sulmachun watershed (8.5 km<sup>2</sup>), which is  
145 a headwater of the Imjin River in northwestern South Korea (Figure 1). The study area is primarily  
146 covered by a mixture of *Polemoniales*, shrubby *Quercus*, and a coniferous canopy of *Pinus*  
147 *densiflora*, with slopes varying between 30° and 45°. Rainfall, streamflow, and other  
148 hydrometeorological records (e.g., temperature and relative humidity) have been collected over  
149 the last 25 years from seven hydrologic monitoring stations in this watershed (Figure 1). The mean  
150 annual rainfall for the last two decades was approximately 1,500 mm; 70% of the total rainfall  
151 occurred during the Asian monsoon season between June and August. Precipitation in the form of  
152 snowfall occurred between December and March. The mean annual evaporation was approximately  
153 420 mm and estimated via eddy-covariance method using data obtained from a flux tower (adjacent  
154 hydrologic monitoring station) located 50 m away from the study area. The average daily  
155 temperature varied between -15°C and 35°C. The hillslope bedrock consists of granite with  
156 extensively weathered areas. Elevations range between 200 and 260 m above sea level, and the  
157 surface slope varies between 20° and 35°. Leptosol and Cambisol (classifications from the Food  
158 and Agricultural Organization of the United Nations) are the dominant soils in the upslope and  
159 downslope areas, respectively. Analysis of 15 soil samples (from 5 points each for the upslope and  
160 downslope areas at depths of 30 cm) indicated that the predominant soil textures were sandy-loam



161 and loamy-sand. The average porosities for the upslope and downslope areas were 49% and 48%,  
162 respectively. Multiple insertions of an iron pole to each grid cell ( $0.5 \times 0.5$  m) indicated that the  
163 soil depth along the hillslope varied between 25 and 95 cm. The depth of the root zone was  
164 approximately 20–30 cm.

165         Rainfall (used to describe rainfall characteristics) was recorded at hourly intervals using a  
166 rainfall gauge (Automatic Rain Gauge System, Eijkelkamp) placed under the canopy. The soil  
167 moisture time series were measured using a multiplex-based time domain reflectometer (TDR;  
168 MiniTRASE, SoilMoisture, 2004) at five locations each for upslope (UP1–UP5) and downslope  
169 (DO1–DO5) (Figure 1). At each location, three TDR sensors (waveguides) were inserted parallel  
170 to the surface at depths of 10, 30, and 60 cm into the upslope side of the installation trench, that  
171 filled with soil. Soil moisture measurements were collected hourly between 2007 and 2016. There  
172 were 356 rainfall events during the study period. A rainfall event was defined by a minimum dry  
173 period of 1 d and at least 1 mm of rainfall.

174

## 175 2.2 Data analysis for soil moisture response

176 For a given rainfall event, the soil moisture variation at a particular point in the hillslope depends  
177 not only on the rainfall but also on other environmental factors such as the location, depth, and soil  
178 texture. To consider the relative variation (%) of water storage normalized by the ASM condition,  
179 we used the soil moisture difference index, which is the percentage of maximum soil moisture  
180 difference (Zhu et al., 2014), to represent the soil moisture variation (VAR):

$$181 \quad \Delta\theta(\%) = \frac{\theta_{max} - \theta_{ant}}{\theta_{ant}} \cdot 100 \quad (4)$$





182 where  $\theta_{max}$  is the maximum soil moisture during a rainfall event and the subsequent period ( $\leq$   
183 4 h), and  $\theta_{ant}$  is the soil moisture measurement before the rainfall event (2 h).

184 We also calculated the time to peak to peak (P2P in h), which is the time difference between the  
185 peak of rainfall and the maximum soil moisture variation. The standard deviation of P2P (SDP2P)  
186 for the measuring points was used to represent the homogeneity of the soil moisture responses  
187 (Kim, 2009). The time series of the soil moisture was converted to address distinct response  
188 features for rainfall events. Depending on soil moisture responses in the transect, location, and  
189 depth, 12 different soil moisture response features were delineated as follows: behavior of all  
190 measurements (total); measurements at upslope points (upslope); and those for downslope  
191 (downslope); measurements for depths of 10 cm (10 cm), 30 cm (30 cm), and 60 cm (60 cm);  
192 measurements for upslope at depths of 10 cm (UP10 cm), 30 cm (UP30 cm), and 60 cm (UP60  
193 cm); measurements for downslope at depths of 10 cm (DO10 cm), 30 cm (DO30 cm), and 60 cm  
194 (DO60 cm).

195

### 196 2.3 Unsupervised Machine Learning Algorithm

197 The SOM utilizes an unsupervised learning algorithm that can be useful for pattern recognition of  
198 multivariate datasets from different observations. The SOM is typically a two-dimensional (2D)  
199 grid composed of either hexagonal or rectangular elements. In this study, we used a hexagonal  
200 lattice as the output layer because it resulted in better information propagation when updating more  
201 neighborhood neurons than that of the rectangular lattice (Kohonen, 2001). Based on the  
202 recommended output dimension of  $5\sqrt{r}$  (Kohonen, 2001), where  $r$  is the number of events, and  
203 the 356 total rainfall events used in this study, the array structure of the SOM was specified as a  
204  $16 \times 6$  matrix, which corresponded to 96 neurons, namely, the grid cells in the SOM. Each neuron



205 had a different weighting vector ( $w_{ab}$ ), where the subscripts  $a$  and  $b$  represent the address codes  
206 for the variable and node, respectively. A random number was used to initialize the weighting  
207 vectors in the neurons. On populating the dataset with rainfall characteristics and soil moisture  
208 data, we can obtain the spatial pattern of SOM (Kohonen, 2001).

209 Input variables for SOM computation were obtained from rainfall features such as rainfall  
210 duration (DUR), rainfall amount (AMO), rainfall intensity (INT), ASM, and maximum soil  
211 moisture difference index to represent VAR and SDP2P for upslope areas at depths of 10, 30, and  
212 60 cm, and those for the downslope area at depths of 10, 30, and 60 cm, respectively. A min-max  
213 transformation was applied to all input variables to fit the bounds of data between zero and one,  
214 except SDP2P, which was  $<1$  in most of the data.

215 SOM maps were established for each variable, and the distance between the input vector  
216 and weighting vector can be calculated as follows:

$$217 \quad d_b = \sqrt{\sum_{a=1}^v (w_{a,b} - x_a)^2}, \quad (5)$$

218 where  $v$  is the number of variables.

219 The best neuron can be identified as the neuron with the minimum value of  $d_b$  indicating  
220 the best fitness to the characteristics of each rainfall event among every neuron in the SOM. Once  
221 the neuron is chosen, the weighting vector should be re-evaluated using Eq. 6 for the renewal  
222 weighting vector as follows:

$$\Delta w_{a,b} = \begin{cases} \alpha(x_a - w_{a,b}) & b = b^* \\ 0 & b \neq b^* \end{cases}$$
$$223 \quad w_{a,b}^{new} = w_{a,b}^{old} + \Delta w_{a,b}, \quad (6)$$



224 where  $\alpha$  ( $= 0.5$ ) is the acceleration coefficient, and  $b^*$  is the winner neuron. Neurons adjacent to  
225 the winner neuron are also updated by applying Eq. (6). The radius of neighboring neurons and  
226 acceleration coefficient decreased linearly (from 16 to 1) as the number of iterations increased.

227 After updating the algorithm, all neurons in the SOM maps fit weighting vectors to the  
228 multiple datasets used in this study. The probability density function of each input variable leading  
229 to selection of specific SOM nodes can then be inferred from the weighting vector. The input  
230 variables in each neuron can be displayed in component planes, which are a spatial pattern in SOM  
231 maps. The nonlinear relationship between variables was identified through visual comparison  
232 between the spatially distributed weightings in each component plane (Adeloye et al., 2011;  
233 Farsadnia et al., 2014; López García and Machón González, 2004; Park et al., 2003).

234

#### 235 2.4 Clustering of Hydrologic events

236 Clusters within the dataset can be delineated by applying the dendrogram classification method  
237 and by evaluating the dissimilarity between the weighting vectors (Montero and Vilar, 2014). We  
238 used a hierarchical method as the resulting dendrogram structure provided a better representation  
239 of the relationships between clusters than the results obtained using non-hierarchical methods. The  
240 hierarchical method forms clusters by binding datasets with shorter distances between them. The  
241 Euclidean distance function was employed to evaluate the dissimilarity as it is suitable for shape-  
242 based comparisons between soil moisture series collected simultaneously (Iglesias and Kastner,  
243 2013). This method has also been used to identify clusters of soil moisture data (Van Arkel and  
244 Kaleita, 2014). The Euclidean distance between two weighting vectors in neurons ( $b_1$  and  $b_2$ ) can  
245 be expressed as follows:

$$246 \quad d_{b_1 b_2} = [\sum_{a=1}^v (w_{a,b_1} - w_{a,b_2})^2]^{0.5}, \quad (7)$$



247 The relationship that has the shortest distance between neurons is assigned to the first cluster, and  
248 the weighting vectors of the first cluster can be expressed as:

$$249 \quad \mu_{c_1,a} = \frac{n_{b_1}\mu_{b_1} + n_{b_2}\mu_{b_2}}{n_{b_1} + n_{b_2}} \quad (8)$$

250 where  $\mu_{b_1}$  and  $\mu_{b_2}$  are the variable weighting vectors in the neurons ( $b_1$  and  $b_2$ ), respectively;  $n_{b_1}$   
251 and  $n_{b_2}$  are set to 1 in this relationship, but these values are set to the number of components during  
252 the comparison of clusters. Additionally, we used Ward's method to evaluate the dissimilarity  
253 between two weighting vectors of each neuron, and between each cluster, namely, this was the  
254 chosen algorithm in our hierarchical clustering method (Ward, 1963). When the dissimilarity  
255 between two clusters ( $c_1$  and  $c_2$ ) is calculated, the distance between clusters can be expressed as:

$$256 \quad d_{cluster} = \sum_{a=1}^v \frac{\|\mu_{a,c_1} - \mu_{a,c_2}\|^2}{\frac{1}{n_{c_1}} + \frac{1}{n_{c_2}}}, \quad (9)$$

257 where  $\mu_{a,c_1}$  and  $\mu_{a,c_2}$  are the averages of clusters  $c_1$  and  $c_2$ , respectively, and  $n_{c_1}$  and  $n_{c_2}$  are the  
258 numbers of components for clusters  $c_1$  and  $c_2$ , respectively. A dendrogram can be constructed  
259 based on the resulting  $d_{cluster}$ , and the upper part from a designated horizontal line can be  
260 recognized as the structure of the final clusters.

261

### 262 **3 Results**

263

#### 264 3.1 Soil moisture responses of all measuring points during rainfall events

265 The statistics of soil moisture response from 30 points are summarized regarding P2P and  
266 maximum variation, as displayed in Fig. 2(a) and 2(b). The P2P ranged from  $-2$  d to  $+4$  d,



267 indicating that the maximum soil moisture can be reached even before the rainfall peak. SDP2P  
268 tends to increase at deeper depths except for locations DO2 and DO5.

269 While the mean P2P for the upslope area was 0.24 d, the downslope area was 0.02 d. Furthermore,  
270 SDP2Ps for upslope and downslope were 0.75 and 0.66 d, respectively. The means of P2P at depths  
271 of 10, 30, and 60 cm were -0.08, 0.04, and 0.011 for the downslope and 0.1, 0.24, and 0.38,  
272 respectively. The difference in P2P between other points at an identical depth for the downslope  
273 was smaller than that for the upslope. This suggests that the soil moisture response in the  
274 downslope area is faster and more uniform than the upslope area. The accumulated soil water flow  
275 from the upslope area to the downslope area appears responsible for quicker and less spatially  
276 variable soil moisture responses in the downslope area. The maximum variation did not display  
277 any notable pattern for the transect to the downslope and the depth profile. This is partially because  
278 the spatial distribution of antecedent moisture is difficult to characterize because of the temporally  
279 varied rainfall event feature and its interaction with the nonlinear soil water process (e.g.,  
280 hysteresis between soil moisture and soil tension).

281

### 282 3.2 Soil moisture responses feature in measuring locations and depths

283 The soil moisture response features (e.g., ASM, maximum variation, and SDP2P) were expressed  
284 in 12 different spatially averaged responses (Fig. 3) depending on the depth and location. As  
285 displayed in Fig. 3(a), the ASM in the downslope area was higher than that in the upslope area. It  
286 is apparent that the deeper the depth, the higher the ASM in the downslope area, but those for the  
287 upslope area did not display any notable trend in the depth profile. This means that soil water  
288 infiltration upslope did not necessarily always occur in all depth profiles.



289 The maximum variation in the downslope area was higher than that of the upslope area, as  
290 displayed in Fig. 3(b). The mean maximum variation in the downslope area (50.67%) was higher  
291 than that of the upslope area (38.73%), and the mean maximum variations at depths of 10, 30, and  
292 60 cm for the upslope area were 44.51%, 34.27%, and 37.39%, while those for the downslope area  
293 were 64.49%, 40.83%, and 46.69%, respectively. This indicates higher wetness along both surface  
294 and subsurface boundaries, and this trend is pronounced in the downslope direction.

295 The SDP2Ps for the 12 soil moisture datasets represent the degree of spatial heterogeneity in the  
296 temporal soil moisture response. The statistics of the SDP2P (Fig. 3(c)) revealed that the  
297 downslope response varied less than that of upslope. While the SDP2P of downslope displayed an  
298 apparent increasing trend at deeper depths, those for upslope were similar in-depth profile. The  
299 difference in the SDP2P profile between the upslope and downslope indicates that the impact of  
300 rainfall on soil moisture response timing can be completely different between upslope and  
301 downslope.

302 The relationships of each response feature (e.g., AMS, VAR, and SDP2P) among different soil  
303 moisture datasets can be visualized through the heat map presented in Fig. 4. The heat map  
304 consisted of coefficients of determination between different soil moisture datasets representing  
305 spatial correlations for different locations, depths, and their combinations. As displayed in Fig. 4,  
306 the heat maps for ASM ranged from 0.88 to 0.99, and those for VAR and SDP2P were from 0.78  
307 to 0.98 and from 0.40 to 0.90, respectively. The relationship between upslope and downslope ( ${}_{2}C_{2}$ ;  
308 namely first combination), those between identical depths ( ${}_{3}C_{2}$ ; namely second combination), and  
309 those for different depths and locations ( ${}_{6}C_{2}$ ; namely third combination) indicate the heterogeneity  
310 of different soil moisture features in the spatial context. The first combinations for ASM, VAR,  
311 and SDP2P were 0.81, 0.72, and 0.53; the means of second and third combinations were 0.95, 0.84,



312 and 0.62, and 0.83, 0.69, and 0.35 for ASM, VAR, and SDP2P, respectively. This suggests that  
313 the spatial distribution of ASM did not demonstrate meaningful spatial variability, but those for  
314 VAR and SDP2P were substantial. Namely, VAR and SDP2P can be useful variables to  
315 characterize the spatial variation of the soil moisture response for the application of SOM.

316

### 317 3.3 Composition and clustering of SOM

318 The dataset of hydrologic measurements ( $356 \times 15$ ) was transformed through 96 neurons and  
319 output regarding a matrix ( $16 \times 6$ ) through the iterative application of Eqs. (5) and (6), respectively:  
320 Namely, 15 hydrologic variables from 356 events were expressed compactly in the SOM.  
321 Dissimilarity regarding the Euclidean distance between the output neurons was then used to  
322 construct the dendrogram. Many alternatives exist in the number of clusters, depending on the  
323 complexity of the dendrogram structure. In this study, five clusters were selected based on a  
324 heuristic approach to achieve a hydrologically meaningful classification of events and  
325 parsimonious clustering. The relation to notable hydrological processes such as lateral flow or  
326 vertical preferential flow and the redundancy check in cluster number were essential factors in the  
327 heuristic approach. Figure 5(a) illustrates the resulting dendrogram for the five clusters. The  
328 structure of the dendrogram demonstrates the relationships between groups of clusters and between  
329 individual clusters. For example, the relationship between clusters 4 and 5 had a lower hierarchy  
330 than clusters 1 and 2. Figure 5(b) presents the output SOM ( $16 \times 6$ ) delineated from the dendrogram  
331 analysis, which is a structural array identical to the delineated dendrogram with neurons for each  
332 cluster. The spatial distributions between other clusters and the corresponding numbers of neurons  
333 indicate the areal portion of each cluster from all clusters and their connections with adjacent  
334 clusters.



335 Table 1 presents the average of vector components, such as the AMO, DUR, INT, and  
336 average ASM among all measuring points (ASMTOT) in volumetric %, alongside an average of  
337 the soil moisture difference indices ( $\Delta\theta$ ) in five upslope locations and five downslope locations at  
338 depths of 10, 30, and 60 cm, as VUP10, VUP30, VUP60, VDO10, VDO30, and VDO60.  
339 Additionally, it presents the SDP2P in five upslope and five downslope locations at depths of 10,  
340 30, and 60 cm, as SUP10, SUP30, SUP60, SDO10, SDO30, and SDO60, respectively, for the five  
341 clusters displayed in Fig. 5(b).

342 As displayed in Figure 5(b), clusters 1 and 2 were in the upper part of the SOM. Table 1  
343 indicates that the rainfall characteristics of clusters 1 and 2, such as DUR, AMO, and INT, were  
344 relatively low, but those for the ASM were similar to the mean ASM for all clusters (Table 1). The  
345 average soil moisture difference indices were less than 5% for cluster 1 because the low AMO and  
346 intensity resulted in a limited increase in soil water storage, and the loss due to evaporation offset  
347 a substantial proportion of the precipitation (Albertson and Kiely, 2001; Ramirez et al., 2007).  
348 Cluster 2 had higher AMO and intensities and more significant average soil moisture differences  
349 than Cluster 1 (Table 1). The intermediate part of the SOM (Figure 5(b)) is associated with Cluster  
350 3, which revealed higher rainfall durations, quantities, and intensities than those for clusters 1 and  
351 2, which resulted in higher soil moisture difference indices for Cluster 3 than for clusters 1 and 2  
352 (Table 1). One notable feature of cluster 3 was the increasing trend of soil moisture difference  
353 indices with depth (DO60 > DO30) for the downslope area, whereas those of clusters 1 and 2  
354 displayed decreased soil moisture difference indices with depth (DO30 > DO60) (Table 1). The  
355 pattern of soil moisture difference indices for Cluster 3 can provide evidence for vertical  
356 infiltration in all depth profiles for upslope and apparent lateral flow downslope (Table 1 and  
357 Figure 4), which appears completely different from those for clusters 1 and 2. Clusters 4 and 5





358 were events demonstrating a larger soil moisture difference index, namely, significant events, in  
359 the SOM classification (Table 1). Cluster 4 displayed two distinctive features compared to the  
360 other clusters. One is that the ASM of cluster 4 was the lowest among all the clusters. However,  
361 the soil moisture difference indices of 30 and 60 cm in the downslope area for Cluster 4 were  
362 significantly higher than those in clusters 1, 2, and 3. The other is that the difference in VAR  
363 between the upslope and downslope is most pronounced in Cluster 4. This means that the  
364 hydrological processes between the upslope and downslope can be substantially distinct from each  
365 other. Both rainfall characteristics and soil moisture difference indices for Cluster 5 were  
366 significantly higher than those for all other clusters. Many of the measurement points in Cluster 5  
367 were saturated during rainfall events, and the soil moisture at a depth of 60 cm displayed higher  
368 variation than that at 30 cm, which indicates that subsurface stormflow was generated along the  
369 bedrock in both the upslope and downslope areas.

370

#### 371 3.4 Component planes for variables

372 The component planes of 16 variables and their visual comparisons can provide insight into the  
373 nonlinear relationships between the 16 hydrological variables. Figure 6 illustrates the SOM  
374 distributions for the component weightings of the 16 variables. Both the spatial distributions and  
375 the scales of weightings (scale bar) in Fig. 6 represent the characteristics of impacts (rainfall  
376 features and ASM) and consequences (average of soil moisture difference and SDP2P).

377 The component planes for AMO, DUR, and INT demonstrate higher weightings in the  
378 lower right part, as displayed in Figs. 6(a)–6(c). The component plane (Fig. 6(d)) for the ASM  
379 displayed lower and higher weightings in the left and right parts. The visual comparison of Figs.  
380 6(a)–6(d) indicates a negligible relationship between rainfall features and ASM. The component



381 planes for upslope soil moisture difference at depths of 10, 30, and 60 cm (Fig. 6(e)–6(g))  
382 displayed similar spatial weightings to those for rainfall features. The high weightings for the soil  
383 moisture difference index at 10 cm depth were mainly distributed to clusters 4 and 5, and the  
384 weightings tended to concentrate in Cluster 5 at deeper depths (Fig. 5). The comparison between  
385 ASM and maximum soil moisture differences indicated that ASM did not influence the VAR index.

386 The exclusive vertical flow impact can be one possible explanation for the relationship  
387 between the component plane for VUP10 and those for VUP30 or VUP60 (Figs. 6(e), 6(f), and  
388 6(g)) because there were negligible upslope contributing areas or small topographic wetness  
389 indices (Fig. 1) in upslope locations. The high weightings of 10 cm for the upslope area were  
390 distributed in two parts of SOM (the lower left and lower right) (Fig. 6(e)), but those of deeper  
391 depths for the upslope area were shifted toward the lower-right part of SOM (Figs. 6(f) and 6(g)).  
392 Weightings in VUP10 were associated with AMO and INT, but those for VUP60 correlated only  
393 with AMO. This pattern of weighting shift was found between VUP30 and VUP60, which can be  
394 attributed to the effect of vertical infiltration (Li et al., 2013). This relationship along the vertical  
395 profile is different between the upslope and downslope. The development of the vertical gradient  
396 in weightings (Figs. 6(e)–6(g)) from VUP10 to VUP60 can hardly be found in weightings from  
397 VDO10 to VDO60 (Figs. 6(h)–6(j)). This means that the flow path in the downslope area cannot  
398 be completely explained by the vertical flow.

399 Figures 6(k)–6(m) displays the component planes of SDP2P at a depth of 10, 30, and 60  
400 cm on the upslope area. The weighting distributions between upslope SDP2P (Figs. 6(k)–6(m))  
401 and ASM (Fig. 6(d)) were completely reverse patterns. The spatial distribution of SDP2P in the  
402 downslope did not reveal a notable difference in-depth profile (Figs. 6(n)–6(p)), which can be  
403 explained by the time to peak in the downslope appearing not only to be determined by the rainfall



404 driver but is more affected by other drivers such as topography. A wider portion of component  
405 planes in the downslope was covered by lower weightings than those for upslope, indicating more  
406 uniform and quicker peak time in the downslope than upslope. Relatively uniform distribution in  
407 peak time matches wetter ASM and vice versa for dry soil moisture conditions.

408

#### 409 **4. Discussion**

##### 410 4.1 Characterization of classified hydrologic event

411 The hydrologic events classified by the SOM can be characterized through comparative feature  
412 presentation for all clusters. Lower ASM matched with a higher mean and wider bound in SDP2P,  
413 which can also be confirmed by the component planes of ASM and SDP2P. The deeper the depth,  
414 the higher the heterogeneity in response time (greater SDP2P) in most locations. This can be  
415 explained by the rainfall control to the soil moisture response time decreasing at deeper depths.  
416 Depending on the cluster, the SDP2P response between the upslope and downslope can be  
417 distinctly expressed. Clusters 1 and 2 exhibited negligible differences in hillslope transects, but  
418 those for clusters 3, 4, and 5 were substantially different. This is because the generation of lateral  
419 flow can be more significant under larger rainfall events at downslope than those for upslope. The  
420 soil moisture peak formations matched well with the maximum variation in soil moisture at the  
421 downslope. Events in cluster 1 demonstrated less variation in SDP2P for both depth profile and  
422 hillslope transact location due to the lowest AMO and INT. The impact of depth on the variation  
423 of SDP2P can be observed in Clusters 2, 3, and 5, and the deeper the depth, the higher the bound,  
424 both upslope and downslope. However, this pattern was different between the upslope and  
425 downslope in Cluster 4, which had the lowest ASM. The lowest ASM leads to substantially less  
426 response variation at 60 cm depth in the upslope, while those for the downslope revealed higher



427 variation at 60 cm depth than those for shallower depths. This means that the dominant flow path  
428 between the upslope and downslope was different in cluster 4.

429 The increasing pattern of the soil moisture difference index corresponds to increasing  
430 rainfall features such as DUR and INT from clusters 1 to 5. However, the depth profile of  
431 maximum VAR was different between clusters 4 and 5. While the scale of soil moisture recharge  
432 demonstrated an apparent decrease in the depth profile for Cluster 4, those for Cluster 5 had  
433 different surface and subsurface boundaries (at depths of 10 and 60 cm). This indicates that the  
434 dominant hydrological processes for Cluster 4 appear restricted to the surface as the vertical flow,  
435 but those for Cluster 5 existed at both the surface and subsurface boundaries regarding both vertical  
436 and lateral flows.

437 The impact of rainfall events on water storage can be useful for understanding the change  
438 in various hydrological statuses for each cluster. The storage changes (Table 2) were estimated by  
439 multiplying the soil moisture change by the corresponding depth for each waveguide (e.g., 200  
440 mm for 10 and 30 cm depths and 300 mm for 60 cm depth). Water storage analysis for Cluster 1  
441 demonstrated negligible changes under 2% (the measurement accuracy of TDR) in soil moisture  
442 that occurred for both the upslope and downslope areas. Rainfall impacts to Cluster 2 can be  
443 classified as an intermediate category because both clusters introduced meaningful storage changes  
444 (mm) in the downslope area. Significant changes in water storage were found for clusters 3, 4, and  
445 5, regardless of the quantity of rainfall. Substantial increases in storage change at a depth of 60 cm  
446 in the downslope area indicated the generation of subsurface stormflow for clusters 3, 4, and 5.  
447 The main difference between clusters 4, 3, and 5 was whether the subsurface lateral flow was  
448 generated in the upslope area. Clusters 3 and 5 can be characterized as high rainfall and high ASM,  
449 which resulted in subsurface lateral flow in both the upslope and downslope areas. The soil



450 moisture changes and storage for cluster 4 indicated an apparent decreasing trend in the depth  
451 profile in the upslope area. The storage changes and soil moisture difference indices at depths of  
452 10 and 30 cm in the upslope area for Cluster 4 were greater than those for Cluster 3 due to higher  
453 AMO, DUR, and INT. However, the storage change at a depth of 60 cm in the upslope for Cluster  
454 4 was smaller than that of Cluster 3, which can be explained by the lower infiltration under drier  
455 ASM conditions (Zhu et al., 2014; Mei et al., 2018; He et al., 2020).

456

#### 457 4.2 Configuration of hydrological processes

458 The application of SOM, an unsupervised machine learning algorithm, to the dataset provided an  
459 integrated assessment to evaluate and characterize hydrologic events. The recharge patterns of  
460 water storage for the soil layers of the hillslope were characterized by several distinct clusters. The  
461 distinct distribution of characteristics of soil moisture responses can be explained by the different  
462 combinations of drivers (rainfall and ASM) and hydrological processes (vertical flow, surface, and  
463 subsurface lateral flows) for each cluster. The hillslope hydrological flow path was characterized  
464 by comparing the component planes between UP10 and UP30 or UP60, and other combinations  
465 of soil moisture component planes, such as those of DO10 and DO30 or DO60 regarding SDP2P  
466 and VAR.

467 The rainfall events can be classified into three distinct categories, which depend on the  
468 rainfall characteristics, and five further refined clusters as follows: insignificant events for Cluster  
469 1, intermediate events for Cluster 2, and significant events for clusters 3, 4, and 5 (Table 3). Further  
470 classification of significant events indicated that the effects of antecedent moisture conditions and  
471 AMO were critical for delineating clusters 3, 5, and 4. The generation of hydrological processes  
472 based on the significant soil moisture changes over 2% and increasing patterns of SDP2P (0.11 for



473 10 cm, 0.18 for 30 cm, and 0.22 for 60 cm depths) at greater depths was the threshold feature  
474 between the insignificant and intermediate events. The primary difference between the  
475 intermediate and significant events was the significant response in both the upslope and downslope  
476 areas and the substantial development of interface flow between the bedrock and soil layer in the  
477 downslope area. This indicates that the lateral flow along boundaries (subsurface and surface) was  
478 stronger than that at intermediate depths, and the downslope lateral flow tended to be generated  
479 through boundaries either along the surfaces or bedrock. Furthermore, ASM was substantially  
480 higher for clusters 3 and 5 than for Cluster 4, and the SDP2D in clusters 3 and 5 were lower for all  
481 points than those for Cluster 4. This can be explained by the development of preferential pipe flow,  
482 which is more common at greater depths under wetter conditions (Lai et al., 2016; Uber et al.,  
483 2018; Uchida et al., 2001; Wienhöfer and Zehe, 2014). Low variation and soil moisture changes  
484 in UP60 for Cluster 4 indicated that low antecedent moisture conditions limit the generation of  
485 lateral flow into the upslope area, and that of Cluster 3 can be explained by even the fewer rainfall  
486 events in Cluster 3 than those for Cluster 4 being sufficient to activate subsurface lateral flow in  
487 the upslope. Extreme rainfall events were mainly associated with Cluster 5. Lateral storm flow  
488 likely occurred in both the upslope and downslope areas of Cluster 5. Effective drainage during  
489 extreme events appears to be strongly associated with lateral flow generation along the two  
490 boundaries in the soil media (i.e., surface and bedrock) (Uchida et al., 2001; Freer et al., 2004;  
491 Haga et al., 2005; Kim, 2009; Wienhöfer and Zehe., 2014; Angermann et al., 2017). The impact  
492 of extreme rainfall conditions dominates other controls (e.g., land cover and topography) regarding  
493 hillslope runoff generation (Feng and Liu, 2015).

494

495



496 **5. Conclusion**

497 Rainfall characteristics and responses of soil moisture at the hillslope scale were explored by  
498 applying SOM to a dataset with a large number of hydrologic events. Hydrologic events were  
499 characterized for rainfall and soil moisture data collected over ten years from a steep hillside.  
500 Based on a delineated dendrogram, the classification of neurons into five clusters provided  
501 meaningful interpretations to understand hydrologic events.

502 The nonlinear relations between hydrologic variables were effectively expressed in the 2D SOM  
503 presentations of variables. The apparent relationship between ASM and peak time variation  
504 indicates that the hydrologic response is more feasible under wetter conditions. Water storage  
505 analysis for each event from different clusters suggests that spatially different combinations of  
506 VAR can be attributed to the identified hydrologic response for each cluster. Combinations of  
507 upslope and downslope spatial patterns of hillslope hydrological processes, vertical flow, and  
508 lateral flow along surface or subsurface boundaries were responsible for the distinctions between  
509 the event clusters. Depending on rainfall and ASM conditions delineated from each cluster, the  
510 spatial distribution of hydrological processes can be predicted to be useful for obtaining systematic  
511 insight into the hillslope hydrological response. The meta-heuristic classification of hydrologic  
512 events provides intuition for hydrologic conditions and their drivers, which is vital for designing a  
513 process-based hillslope hydrology model.

514

515

516

517

518

519



520 **Code and Data Availability**

521 Code will be available through repository <https://www.re3data.org/> when paper is accepted. Data  
522 is uploaded as supplementary materials.

523

524 **Author contribution**

525 Enhyung Lee and Sanghyun Kim and several former graduate students had collected data for the  
526 study area. Eunhyung Lee developed model code and performed simulation. Sanghyun Kim  
527 prepared manuscript with contribution from Enhyung Lee.

528

529 **Competing interests**

530 The authors declare that they have no conflict of interest

531

532 **Acknowledgments**

533 This study was financially supported by the Basic Research Program (2016R1D1A1B02008137)  
534 of the National Science Foundation of the Republic of Korea.

535

536 **References**

- 537 Adeloje, A. J., Rustum, R., and Kariyama, I.D.: Kohonen self-organizing map estimator for the  
538 reference crop evapotranspiration, *Water Resour. Res.*, 47(8),  
539 <https://doi.org/10.1029/2011WR010690>, 2011.
- 540 Ahmad, S., Kalra, A., and Stephen, H.: Estimation soil moisture using remote sensing data: A  
541 machine learning approach, *Adv. Water Resour.*, 33(1), 69-80,  
542 <https://doi.org/10.1016/j.advwatres.2009.10.008>, 2010.
- 543 Albertson, J. D., and Kiely, G.: On the structure of soil moisture time series in the context of land  
544 surface models, *J. Hydrol.*, 243, 101-119, [https://doi.org/10.1016/S0022-1694\(00\)00405-](https://doi.org/10.1016/S0022-1694(00)00405-4)  
545 4, 2001.





- 546 Ali, M., Fiori, A., and Bellotti, G.: Analysis of the nonlinear storage-discharge relation for  
547 hillslopes through 2D numerical modelling, *Hydrol. Process.*, 27, 2683-2690,  
548 <https://doi.org/10.1002/hyp.9397>, 2013.
- 549 Angermann, L., Jackish, C., Allroggen, N., Sprenger, M., Zehe, E., Tronicke, J., Weiler, M., and  
550 Blume, T.: Form and function in hillslope hydrology: characterization of subsurface flow  
551 based on response observations, *Hydrol. Earth Syst. Sci.*, 21, 3727-3748,  
552 <https://doi.org/10.5194/hess-21-3727-2017>, 2017.
- 553 Bachmair, S., Weiler, M., and Troch, P. A.: Intercomparing hillslope hydrological dynamics:  
554 Spatio-temporal variability and vegetation cover effects, *Water Resour. Res.*, 48,  
555 W05537, <https://doi.org/10.1029/2011WR011196>, 2012.
- 556 Baroni, G., Ortuani, B., Facchi, A., and Gandolfi, C.: The role of vegetation and soil properties  
557 on the spatio-temporal variability of the surface soil moisture in a maize-cropped field, *J.*  
558 *Hydrol.*, 489, 148-159, <https://doi.org/10.1016/j.jhydrol.2013.03.007>, 2013.
- 559 Carranza, C., Nolet, C., Pejjij, M., Ploeg, and van der Ploeg, M.: Root zone soil moisture  
560 estimation with random forest, *J. Hydrol.*, 593, 125840,  
561 <https://doi.org/10.1016/j.jhydrol.2020.125840>, 2021.
- 562 Casper, M.C., Grigoryan, G., Gronz, O., Gutjahr, O., Heinemann, G., Ley R., and Rock, A.:  
563 Analysis of projected hydrological behavior of catchments based on signature indices,  
564 *Hydrol. Earth Syst. Sci.*, 16, 409-421, <https://doi.org/10.5194/hess-16-409-2012>, 2012.
- 565 Castillo, V.M., Gomez-Plaza, A., and Martinez-Mena, M.: The role of antecedent soil water  
566 content in the runoff response of semiarid catchments: a simulation approach, *J.*  
567 *Hydrology*, 284(1-4), 114-130, [https://doi.org/10.1016/S0022-1694\(03\)00264-6](https://doi.org/10.1016/S0022-1694(03)00264-6), 2003.
- 568 Chen, I.T., Chang, L.C., and Chang, F.J.: Exploring the spatio-temporal interrelation between  
569 groundwater and surface water by using the self-organizing maps, *J. Hydrol.*, 556, 131-  
570 142, <https://doi.org/10.1016/j.jhydrol.2017.10.015>, 2018.
- 571 Crow, W.T., and Ryu, D.: A new data assimilation approach for improving runoff prediction  
572 using remotely-sensed soil moisture retrievals, *Hydrol. Earth Syst. Sci.*, 13, 1-16,  
573 <https://doi.org/10.5194/hess-13-1-2009>, 2009.
- 574 Curtu, R., Mantilla, R., Fonley, M., Cunha, L.K., Small, S.J., Jay, L.O., and Krajewski, W.F.: An  
575 integral-balance nonlinear model to simulate changes in soil moisture, groundwater and  
576 surface runoff dynamics at the hillslope scale, *Adv. Water Resour.*, 71, 125-139,  
577 <https://doi.org/10.1016/j.advwatres.2014.06.003>, 2014.
- 578 di Prinzio, M., Cstellarin, A., and Toth, E.: Data-driven catchment classification: application to  
579 the pub problem, *Hydrol. Earth Syst. Sci.*, 15, 1921-1935, <https://doi.org/10.5194/hess-15-1921-2011>, 2011.
- 581 Farsadnia, F., Kamrood, M. R., Nia, A. M., Modarres, R., Bray, M. T., Han, D., and Sadatinejad,  
582 J.: Identification of homogeneous regions for regionalization of watersheds by two-level  
583 self-organizing feature maps, *J. Hydrol.*, 509, 387-397,  
584 <https://doi.org/10.1016/j.jhydrol.2013.11.050>, 2014.
- 585 Gwak, Y., Kim, S., Factors affecting soil moisture spatial variability for a humid forest hillslope,  
586 *Hydrolo. Process.* 31(2), 431-445, <https://doi.org/10.1002/hyp.11039>, 2016



- 587 Feng, H., and Liu, Y.: Combined effects of precipitation and air temperature on soil moisture in  
588 different land covers in a humid basin, *J. Hydrol.*, 531, 1129-1140,  
589 <https://doi.org/10.1016/j.jhydrol.2015.11.016>, 2015.
- 590 Freer, J., McDonnell, J., Beven, K., Peters, N. E., Burns, D. A., Hooper, R. P., Aulenbach, B.,  
591 and Kendall, C.: The role of bedrock topography on subsurface storm flow, *Water*  
592 *Resour. Res.*, 38(12), W1269, <https://doi.org/10.1029/2001WR000872>, 2004.
- 593 Haga, H., Matsumoto, Y., Matsutani, J., Fujita, M., Nishida, K., and Sakamoto, Y.: Flow paths,  
594 rainfall properties, and antecedent soil moisture controlling lags to peak discharge in a  
595 granitic unchanneled catchment, *Water Resour. Res.*, 41, W12410,  
596 <https://doi.org/10.1029/2005WR004236>, 2005.
- 597 Hardie, M.A., Cotching, W.E., Doyle, R.B., Holz, G., Lisson, S., and Mattern, K.: Effect of  
598 antecedent soil moisture on preferential flow in a texture-contrast soil, *J. Hydrol.*, 398(3-  
599 4), 191-201, <https://doi.org/10.1016/j.jhydrol.2010.12.008>, 2011.
- 600 He, Z., Jia, G., Liu, Z., Zhang, Z., Yu, X., and Xiao, P.: Field studies on the influence of rainfall  
601 intensity, vegetation cover and slope length on soil moisture infiltration on typical  
602 watersheds of the Loess Plateau, China, *Hydrol. Process.*, 34, 4904-4919,  
603 <https://doi.org/10.1002/hyp.13892>, 2020.
- 604 He, Z., Zhao, W., Liu, H., and Chang, X.: The response of soil moisture to rainfall event size in  
605 subalpine grassland and meadows in a semi-arid mountain range: a case study in  
606 northwestern China's Qilian Mountains, *J. Hydrol.*, 420-421, 183-190,  
607 <https://doi.org/10.1016/j.jhydrol.2011.11.056>, 2012.
- 608 Heisler-White, J. L., Knapp, A. K., and Kelly, E. F.: Increasing precipitation event size increases  
609 aboveground net primary productivity in a semi-arid grassland, *Oecologia*, 158, 129-140,  
610 <https://doi.org/10.1007/s00442-008-1116-9>, 2008.
- 611 Herbst, M., Gupta, H.V., and Casper, M.C.: Mapping model behavior using self-organizing  
612 maps, *Hydrol. Earth Syst. Sci.*, 13, 395-409, <https://doi.org/10.5194/hess-13-395-2009>,  
613 2009.
- 614 Iglesias, F., and Kastner, W.: Analysis of similarity measures in times series clustering for the  
615 discovery of building energy patterns, *Energies*, 6, 579-597,  
616 <https://doi.org/10.3390/en6020579>, 2013.
- 617 Ismail, S., Shabri, A., and Samsudin, R.: A hybrid model of self organizing maps and least  
618 square support vector machine for river flow forecasting, *Hydrol. Earth Syst. Sci.*, 16,  
619 4417-4443, <https://doi.org/10.5194/hess-16-4417-2012>, 2012.
- 620 Kim, S.: Characterization of soil moisture responses on a hillslope to sequential rainfall events  
621 during late autumn and spring, *Water Resour. Res.* 45, W09425, <https://doi.org/10.1029/2008WR007239>, 2009.
- 623 Kohonen, T.: *Self-Organizing Maps*, third ed., Springer, Berlin, 2001.
- 624 Lai, X., Liao, K., Feng, H., and Zhu, Q.: Responses of soil water percolation to dynamic  
625 interactions among rainfall, antecedent moisture and season in forest site, *J. Hydrol.*, 540,  
626 565-573, <https://doi.org/10.1016/j.jhydrol.2016.06.038>, 2016.



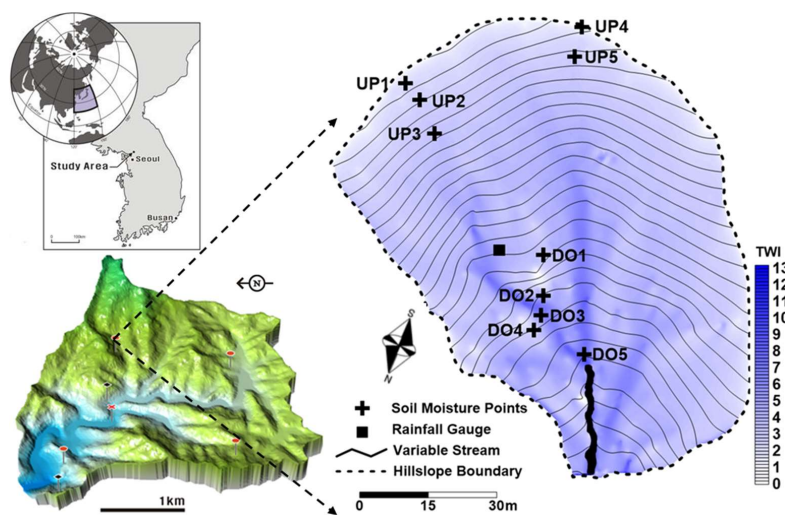
- 627 Lee, E. and Kim, S.: Pattern similarity based soil moisture analysis for three seasons on a steep  
628 hillslope, *J. Hydrol.*, 551, 484-494, <https://doi.org/10.1016/j.jhydrol.2017.06.028>, 2017.
- 629 Lee E., and Kim, S.: Characterization of runoff generation in a mountainous hillslope according  
630 to multiple threshold behavior and hysteretic loop features, *J. Hydrol.*, 590, 125534,  
631 <https://doi.org/10.1016/j.jhydrol.2020.125534>, 2020.
- 632 Ley, R., Casper, M. C., Hellebrand, H., and Merz, R.: Catchment classification by runoff  
633 behavior with self-organizing maps (SOM), *Hydrol. Earth Syst. Sci.*, 15, 2947-2962,  
634 <https://doi.org/10.5194/hess-15-2947-2011>, 2011.
- 635 Li, X. Y., Zhang, S. Y., Peng, H. Y., Hu, X., and Ma, Y. J.: Soil water and temperature dynamics  
636 in shrub-encroached grasslands and climatic implications: Results from inner Mongolia  
637 steppe ecosystem of north China, *Agric.For.Meteorol.*, 171, 20-30,  
638 <https://doi.org/10.1016/j.agriformet.2012.11.001>, 2013.
- 639 Liang, W. L., Kosugi, K., and Mizuyama, T.: Soil water dynamics around a tree on a hillslope  
640 with or without rainwater supplied by stemflow, *Water Resour. Res.*, 47, W02541,  
641 <https://doi.org/10.1029/2010WR009856>, 2011.
- 642 Liao, K., Zhou, Z., Lai, X., Zhu, Q., and Feng, H.: Evaluation of different approaches for  
643 identifying optimal sites to predict mean hillslope soil moisture content, *J. Hydrol.*, 547,  
644 10-20, <https://doi.org/10.1016/j.jhydrol.2017.01.043>, 2017.
- 645 López García, H., and Machón González, I.: Self-organizing map and clustering for wastewater  
646 treatment monitoring, *Engineering Application of Artificial Intelligence*, 17, 215-225,  
647 <https://doi.org/10.1016/j.engappai.2004.03.004>, 2004.
- 648 Lu, N., and Godt, J.: Infinite slope stability under steady unsaturated seepage conditions, *Water  
649 Resour. Res.*, W11404, <https://doi.org/10.1029/2008WR006976>, 2008.
- 650 Mei, X., Zhu, Q., Ma, L., Zhang, D., Wang, Y., and Hao, W.: Effect of stand origin and slope  
651 position on infiltration pattern and preferential flow on a Loess hillslope, *Land Degrad.  
652 Dev.*, 29, 1353-1365, <https://doi.org/10.1002/ldr.2928>, 2018.
- 653 Montero, P., and Vilar, J.A.: TSclust: An R package for time series clustering, *J. Stat. Softw.*,  
654 62(1), 1-43, <https://doi.org/10.18637/jss.v062.i01>, 2014
- 655 Park, Y. S., Cereghino, R., Compin, A., and Lek, S.: Applications of artificial neural networks  
656 for patterning and predicting aquatic insect species richness in running waters, *Ecol  
657 Model.*, 160, 265-280, [https://doi.org/10.1016/S0304-3800\(02\)00258-2](https://doi.org/10.1016/S0304-3800(02)00258-2), 2003.
- 658 Penna, D., Borga, M., Norbiato, D., and Fontana, G. D.: Hillslope scale soil moisture variability  
659 in a steep alpine terrain, *J. Hydrol.*, 364, 311-327,  
660 <https://doi.org/10.1016/j.jhydrol.2008.11.009>, 2009.
- 661 Penna, D., Tromp van Meerveld, H. J., Gobbi, A., Borga, M., and Fontana, G. D.: The influence  
662 of soil moisture on threshold runoff generation processes in an alpine headwater  
663 catchment, *Hydrol. Earth Syst. Sci.*, 15, 689-702, [https://doi.org/10.5194/hess-15-689-  
664 2011](https://doi.org/10.5194/hess-15-689-2011), 2011.
- 665 Ramirez, D. A., Bellot, J., Domingo, F., and Blasco, A.: Can water responses in *stipa tenacissima*  
666 L. during the summer season be promoted by non-rainfall water gains in soil?, *Plant and  
667 Soil*, 291, 67-79, <https://doi.org/10.1007/s11104-006-9175-3>, 2007.



- 668 Rodriguez-Iturbe, I., Isham, V., Cox, D. R., Manfreda, S., and Porporato, A.: Space-time  
669 modeling of soil moisture: Stochastic rainfall forcing with heterogeneous vegetations,  
670 *Water Resour. Res.*, 42, W06D05, <https://doi.org/10.1029/2005WR004497>, 2006.
- 671 Rosenbaum, U., Bogen, H. R., Herbst, M., Huisman, J. A., Peterson, T. J., Weuthen, A.,  
672 Western, A. W., and Vereecken, H.: Seasonal and event dynamics of spatial soil moisture  
673 patterns at the small catchment scale, *Water Resour. Res.*, 48, W10544,  
674 <https://doi.org/10.1029/2011WR011518>, 2012.
- 675 Saffarpour, S., Western, A.W., Adams, R., and McDonnell, J.J.: Multiple runoff processes and  
676 multiple thresholds control agricultural runoff generation, *Hydrol. Earth Syst. Sci.*, 20,  
677 4525-4545, <https://doi.org/10.5194/hess-20-4525-2016>, 2016.
- 678 Shrestha, D.L., Kayastha, N., and Solomatine, D.P.: A novel approach to parameter uncertainty  
679 analysis of hydrological models using neural networks, *Hydrol. Earth Syst. Sci.*, 13,  
680 1235-1248, <https://doi.org/10.5194/hess-13-1235-2009>, 2009.
- 681 Srivastava, P.K., Han, D., Ramirez, M.R., and Islam, T.: Machine learning techniques for  
682 downscaling smos satellite soil moisture using modis land surface temperature for  
683 hydrological application, *Water Resour. Manag.*, 27, 3127-3144,  
684 <https://doi.org/10.1007/s11269-013-0337-9>, 2013.
- 685 Toth, E.: Catchment classification based on characterization of streamflow and precipitation time  
686 series, *Hydrol. Earth Syst. Sci.*, 17, 1149-1159, [https://doi.org/10.5194/hess-17-1149-](https://doi.org/10.5194/hess-17-1149-2013)  
687 2013, 2013.
- 688 Tromp van Meerveld, I., and McDonnell, J.J.: Comment to “Spatial correlation of soil moisture  
689 in small catchments and its relationship to dominant spatial hydrological processes,  
690 *J.Hydrol.*, 286, 113-134”, *J.Hydrol.*, 303, 307-312,  
691 <https://doi.org/10.1016/j.jhydrol.2004.09.002>, 2005.
- 692 Trambly, Y., Bouaicha, R., Brocca, L., Dorigo, W., Bouvier, C., Camici, S., and Servat, E.:  
693 Estimation of antecedent wetness conditions for flood modelling in northern morocco,  
694 *Hydrol. Earth Syst. Sci.*, 16, 4375-4386, <https://doi.org/10.5194/hess-16-4375-2012>,  
695 2012.
- 696 Uber, M., Vandervaere, J.P., Zin, I., Braud, I., Heistermann, M., Legout, C., Molinie, G., and  
697 Nord, G.: How does initial soil moisture influence the hydrological response? A case  
698 study from southern france, *Hydrol. Earth Syst. Sci.*, 22, 6127-6146,  
699 <https://doi.org/10.5194/hess-22-6127-2018>, 2018.
- 700 Uchida, T., Kosugi, K., and Mizuyama, T.: Effects of pipeflow on hydrological process and its  
701 relations to landslide, a review of pipeflow studies in forested headwater catchments,  
702 *Hydrol. Process.* 15, 2151-2174, <https://doi.org/10.1002/hyp.281>, 2001.
- 703 Van Arkel, Z., and Kaleita, A. L.: Identifying sampling locations for field-scale soil moisture  
704 estimation using K-means clustering. *Water Resour. Res.* 50 (8), 7050-7057,  
705 <https://doi.org/10.1002/2013WR015015>, 2014.
- 706 Wang, S., Fu, B., Gao, G., Liu, Y., and Zhou, J.: Responses of soil moisture in different land  
707 cover types to rainfall events in a re-vegetation catchment area of the Loess Plateau,  
708 *China, Catena*, 101, 122-128, <https://doi.org/10.1016/j.catena.2012.10.006>, 2013.



- 709 Wang, X. P., Cui, Y., Pan, Y. X., Li, X. R., Yu, Z., and Young, M. H.: Effects of rainfall  
710 characteristics on infiltration and redistribution patterns in revegetation-stabilized desert  
711 ecosystems, *J. Hydrol.*, 358, 134-143, <https://doi.org/10.1016/j.jhydrol.2008.06.002>,  
712 2008.
- 713 Western, A. W., Grayson, R. B., Blöschl, G. Willgoose, G. R., McMahon, T. A., Observed  
714 spatial organization of soil moisture and its relation to terrain indices, *Water Resour.*  
715 *Res.*, 35(3), 797-8110, <https://doi.org/10.1029/1998WR900065>, 1999.
- 716 Wiekenkamp, I., Huisman, J.A., Bogena, H.R., Lin, H.S., and Vereecken, H.: Spatial and  
717 temporal occurrence of preferential flow in a forested headwater catchment, *J. Hydrol.*,  
718 534, 139-149, <https://doi.org/10.1016/j.jhydrol.2015.12.050>, 2016.
- 719 Wienhöfer, J., and Zehe, E.: Predicting subsurface stormflow response of a forested hillslope: the  
720 role of connected flow paths, *Hydrol. Earth Syst. Sci.*, 18, 121-138,  
721 <http://doi.org/10.5194/hess-18-121-2014>, 2014.
- 722 Wilson, D. J., Western, A. W., and Grayson, R. B.: Identifying and quantifying sources of  
723 variability in temporal and spatial soil moisture observations, *Water Resour. Res.*, 40,  
724 W02507, <https://doi.org/10.1029/2003WR002306>, 2004.
- 725 Zhang, Y., Wei, H., and Nearing M.A.: Effects of antecedent soil moisture on runoff medeling in  
726 small semiarid watersheds of southeastern Arizona, *Hydrol. Earth Syst. Sci.*, 15, 3171-  
727 3179, <https://doi.org/10.5194/hess-3171-2011>, 2011.
- 728 Zhu, Q., Nie, X. F., Zhou, X. B., Liao, K. H., and Li, H. P.: Soil moisture response to rainfall at  
729 different topographic positions along a mixed land-use hillslope, *Catena*, 119, 61-70,  
730 <https://doi.org/10.1016/j.catena.2014.03.010>, 2014.
- 731  
732  
733  
734  
735  
736  
737  
738  
739  
740  
741



742

743 **Figure 1.** Location of Sulmachun watershed in South Korea with hydrologic monitoring (rainfall  
744 and evapotranspiration) stations (lower left) and study area with terrain contours, topographic  
745 wetness index (TWI), and soil moisture monitoring points (right). (We created this map)

746

747

748

749

750

751

752

753

754

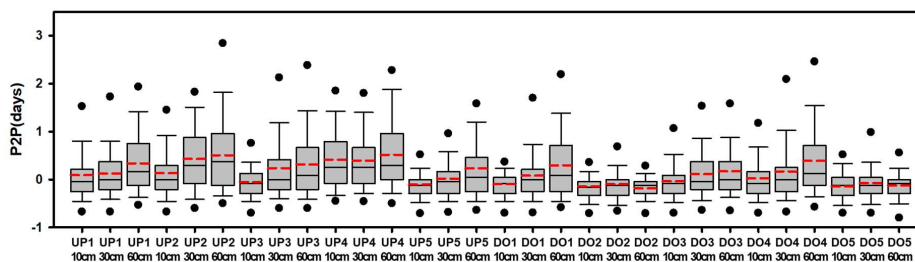
755

756

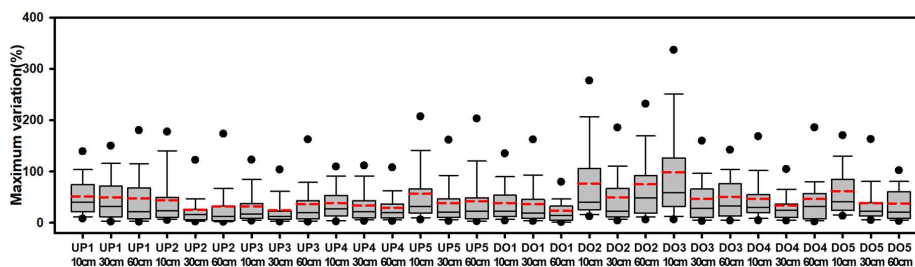
757

758

759



(a)



(b)

760 **Figure 2** Boxplots of soil moisture responses of P2P (a) and maximum variation (b) for 30  
761 points.

762  
763  
764  
765  
766  
767  
768  
769  
770  
771

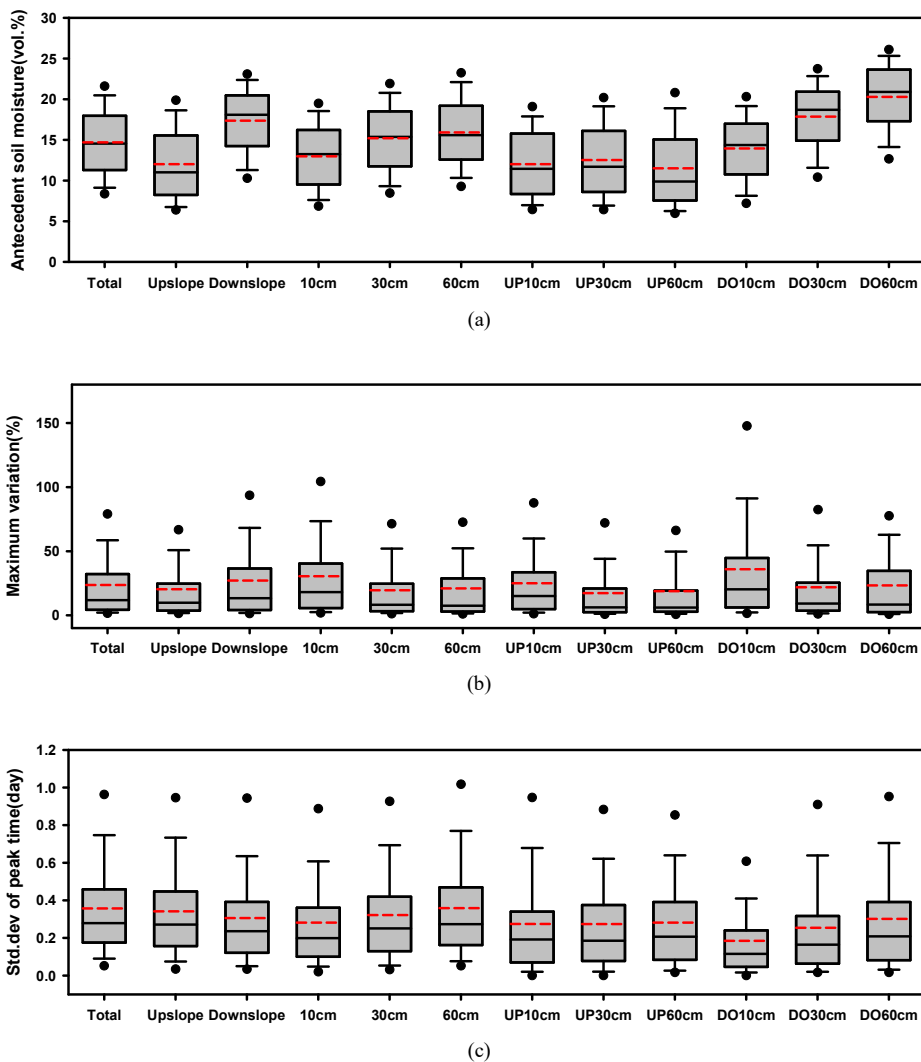


**Figure 3** Box plots of antecedent soil moisture (a), maximum variation (b), and standard deviation of peak time (SDP2P) (c) of 12 time series of soil moistures.

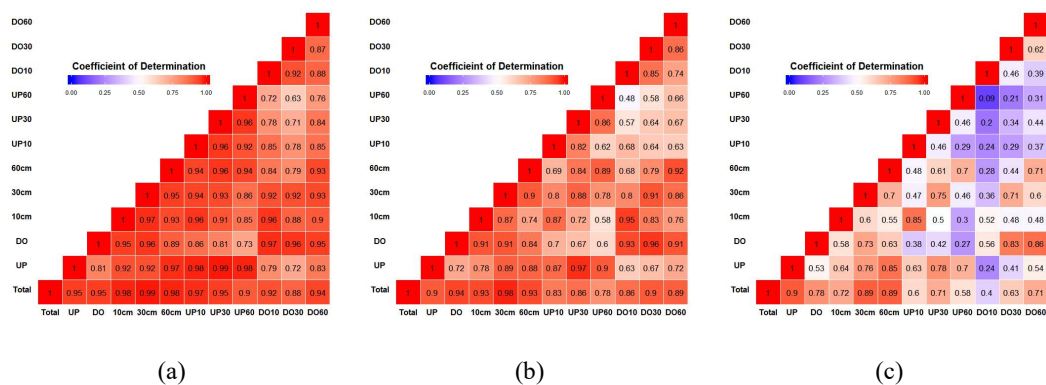
772  
773  
774  
775  
776  
777  
778





779

780



781 **Figure 4.** Heat maps of coefficient of determination among combinations of (a) antecedent soil  
 782 moisture, (b) maximum variation, (c) standard deviation of peak time.

783

784

785

786

787

788

789

790

791

792

793

794

795

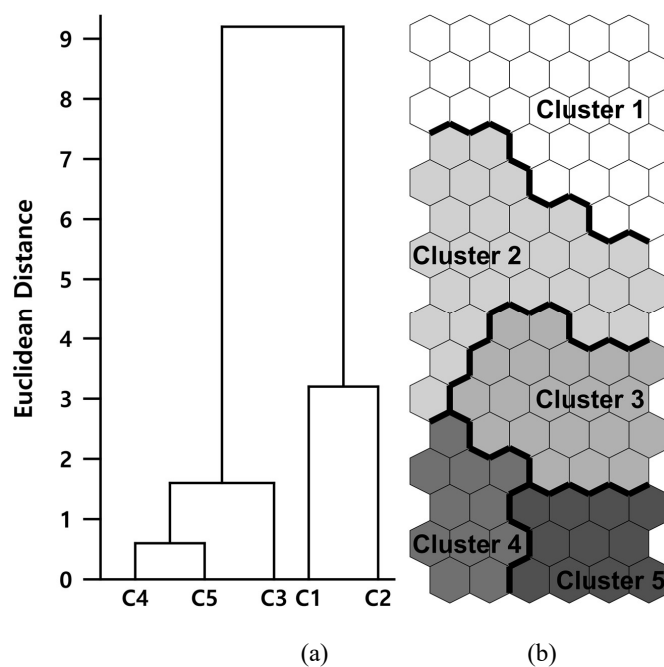
796

797

798

799

800



801

802

803 Figure 5. Structure of (a) dendrogram for five clusters and (b) SOM classifications in 96 neurons  
804 through  $16 \times 6$  matrix.

805

806

807

808

809

810

811

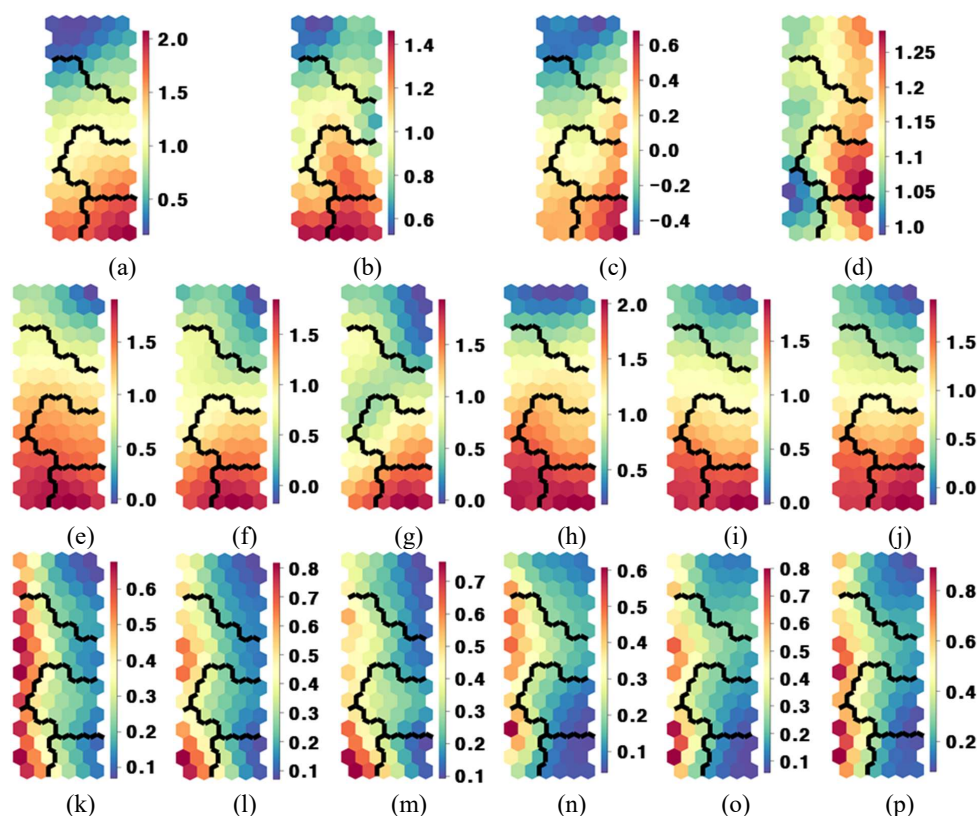
812

813

814

815

816



817 **Figures 6.** (a)–(p) Component planes of variable weightings for rainfall amount (AMO) (a);  
818 rainfall duration (DUR) (b); rainfall intensity (INT) (c); antecedent soil moisture (ASM) (d); soil  
819 moisture difference indices for the upslope and downslope at depths of 10, 30, and 60 cm (VUP10,  
820 VUP30, VUP60, VDO10, VDO30, VDO60) (e)–(j); standard deviation of peak time for the  
821 upslope and downslope at depths of 10, 30, and 60 cm (SUP10, SUP30, SUP60, SDO10, SDO30,  
822 and SDO60) (k)–(p)

823

824

825

826

827

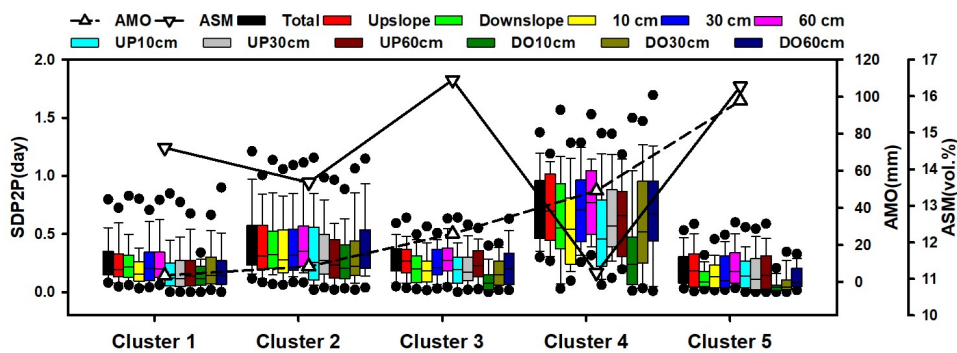
828

829

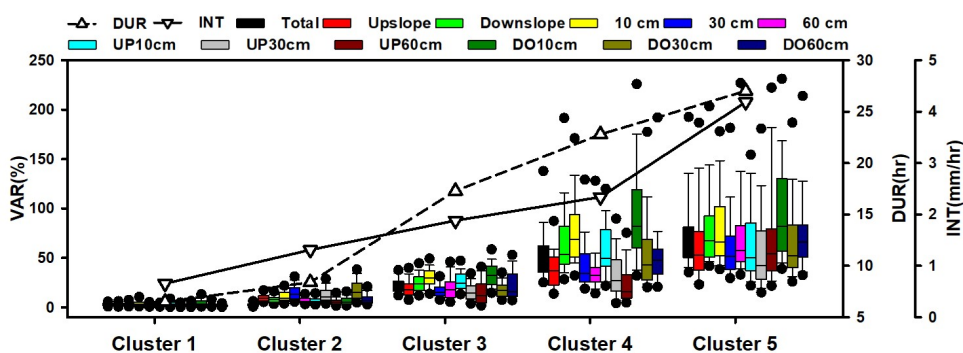
830



831



(a)



(b)

832 Figure 7. SDP2Ps with mean AMO and ASM for each cluster (a) soil moisture difference index  
 833 with mean DUR and INT for each cluster for total, upslope, and downslope at depths of 10, 30,  
 834 and 60 cm, corresponding depths for upslope and downslope.

835

836

837

838

839

840



841

842 Table 1. Arithmetic averages of SOM inputs for rainfall amount (AMO), rainfall duration (DUR),  
 843 rainfall intensity (INT), antecedent soil moisture for all points (ASMTOT), maximum soil  
 844 moisture variation (VAR), and standard deviation of peak-to-peak time (SDP2P).

Variables	numbers	AMO(mm)	DUR(hr)	INT(mm/hr)	ASMTOT(vol.%)	
cluster 1	108	3.61	6.50	0.66	14.6	
cluster 2	90	8.45	8.40	1.31	13.6	
cluster 3	75	26.08	17.28	1.88	16.4	
cluster 4	30	49.27	22.80	2.34	11.2	
cluster 5	53	97.80	27.02	4.19	16.3	
VAR(%)	VUP10	VUP30	VUP60	VDO10	VDO30	VDO60
cluster 1	3.8	2.0	2.5	4.6	2.9	1.9
cluster 2	13.2	5.7	6.8	17.5	8.6	7.2
cluster 3	26.9	16.4	16.1	33.4	18.2	22.9
cluster 4	59.1	33.0	23.4	96.1	56.6	54.8
cluster 5	66.7	60.8	73.9	100.7	68.6	77.4
SDP2P	SUP10	SUP30	SUP60	SDO10	SDO30	SDO60
cluster 1	0.21	0.20	0.21	0.16	0.22	0.22
cluster 2	0.37	0.35	0.33	0.30	0.35	0.42
cluster 3	0.22	0.22	0.26	0.11	0.18	0.22
cluster 4	0.56	0.65	0.63	0.36	0.59	0.72
cluster 5	0.17	0.17	0.20	0.06	0.09	0.12

845

846

847

848

849

850

851

852

853

854



855

856 Table 2. Soil moisture changes and storage changes for all clusters at depths of 10 cm, 30 cm, and  
 857 60 cm and those for upslope and downslope.

average	cluster	10cm	30cm	60cm	upslope			downslope		
					10cm	30cm	60cm	10cm	30cm	60cm
soil moisture change (%)	1	0.5	0.4	0.3	0.4	0.3	0.3	0.6	0.5	0.4
	2	1.9	1.0	1.0	1.5	0.6	0.7	2.3	1.5	1.4
	3	4.5	2.9	3.5	3.7	2.4	2.1	5.2	3.5	5.1
	4	7.4	5.2	4.9	5.3	3.1	2.0	9.8	7.8	9.0
	5	12.0	10.8	13.3	8.9	8.7	10.0	15.4	13.3	16.8
storage change (mm)	1	1.0	0.8	0.9	0.8	0.6	0.9	1.2	1.0	1.2
	2	3.8	2.0	3.0	3.0	1.2	2.1	4.6	3.0	4.2
	3	9.0	5.8	10.5	7.4	4.8	6.3	10.4	7.0	15.3
	4	14.8	10.4	14.7	10.6	6.2	6.0	19.6	15.6	27.0
	5	24.0	21.6	39.9	17.8	17.4	30.0	30.8	26.6	50.4

858

859

860

861

862

863

864

865

866

867

868



869 Table 3. Combinations of flow paths and its hydrologic conditions for all clusters.  
 870 SF: surface; SB: subsurface.  
 871

Cluster	#	Rainfall Impact	Antecedent	Upslope		Downslope	
			soil moisture	Vertical flow	Lateral flow	Vertical flow	Lateral flow
				SF/SB		SF/SB	
1	108	Insignificant	Mid	No response (under 2 vol.%)		No response (under 2 vol.%)	
2	90	Intermediate	Mid	No response (under 2 vol.%)		Yes	No
3	30		High	Yes	No/Yes	Yes	No/Yes
4	53	Significant	Low	Yes	No/No	Yes	No/Yes
5	75		High	Yes	No/Yes	Yes	Yes/Yes